NASA Technical Memorandum 86814

Comparison of Measured Temperatures, Thermal Stresses and Creep Residues With Predictions on a Built-up Titanium Structure

Jerald M. Jenkins

November 1987

NASA
National Aeronautics and
Space Administration

Comparison of Measured Temperatures, Thermal Stresses and Creep Residues With Predictions on a Built-up Titanium Structure

Jerald M. Jenkins
Ames Research Center, Dryden Flight Research Facility, Edwards, California

1987

NASA

SUMMARY

Temperature, thermal stresses, and residual creep stresses were studied by comparing laboratory values measured on a built-up titanium structure with values calculated from finite-element models. A two-dimensional finite-element thermal model, including conduction, radiation, and convection heat transfer, was developed that predicted laboratory-measured transient temperatures quite well. The emissivity and convective film coefficient were adjusted to empirical data to refine the thermal model.

Several finite-element models were used to examine the relationship between computational thermal stresses and thermal stresses measured on a built-up test structure. Element suitability, element density, and computational temperature discrepancies were studied to determine their impact on measured and calculated thermal stress. Both bar and plate elements were found suitable for the uniaxial stress situation of this built-up test structure. The number of elements in the web area of the spar was critical to accurate thermal stress calculation. The optimum number of elements is established from a balance between element density and suitable safety margins, such that the answer is acceptably safe yet is economical from a computational viewpoint. Since the computed temperature discrepancies were generally quite small, the difference between thermal stresses computed with measured temperatures and with computed temperatures was also quite small. It was noted situations exist where relatively small excursions of calculated temperatures from measured values result in far more than proportional increases in thermal stress values.

Measured residual stresses due to creep significantly exceeded the values computed by the piecewise linear inelastic strain analogy approach. The most important element in the computation is the correct definition of the creep law. Available literature revealed such a wide variety of viscoelastic properties that the creep law is considered the major contributor to the discrepancy. Computational methodology advances in predicting residual stresses due to creep require significantly more viscoelastic material characterization than is currently available.

INTRODUCTION

Creep is a primary limiting factor in metal alloy application to elevated temperature structural situations. Frequently, an alloy that meets strength, weight, and stiffness requirements at elevated temperature may not have acceptable creep performance (refs. 1 to 3). The adverse effects of creep may occur as excessive deformations, residual stresses, or failure. The many ways in which creep effects may manifest requires that (1) creep be predictable in built-up structures or (2) the environment resulting in creep be avoided. The latter option may be a very expensive retreat in terms of weight for many contemplated aeronautical or space concepts.

This paper presents the experimental results of a laboratory test in which a built-up test structure of titanium was heated and loaded to conditions that would result in creep. The residual stresses resulting from creep were measured using strain gages. An approach to predicting creep-induced residues was implemented using an existing finite-element computer program. Creep residues were computed and compared to measured residuals. Temperatures and thermal stresses were also measured and compared to predictions.

NOMENCLATURE

CBAR	bar element
CHEXA2	three-dimensional element
CQUAD2	quadrilateral plate element
CROD	rod element
CSHEAR	shear element
CTRIA2	triangular plate element
E	Young's modulus, lb/in^2
G	shear modulus, lb/in^2
h	thickness, in
i, j, m	integers
NASTRAN	NASA structural analysis
T	temperature, °F
t	time, hr
y/d	depth ratio, in/in
α	coefficient of thermal expansion, in/in °F
δ_{ij}	Kronecker delta
ϵ	strain, in/in
ϵ_{ij}	total strain, in/in
ϵ'_{ij}	elastic strain, in/in
ϵ''_{ij}	inelastic strain, in/in
ν	Poisson's ratio
σ	stress, lb/in^2

Subscripts:

i, j, m	integers
C	creep
P	plasticity
T	temperature
TC	composite of temperature and creep

DESCRIPTION OF TEST SPECIMEN AND INSTRUMENTATION

A cross-sectional drawing of the test specimen is presented in figure 1. The specimen is typically a skin-substructure type of structure. The 0.25-in-thick skin, the 0.050-in-substructure frames, and the 0.45-in frame caps were all constructed of titanium alloy 6A1-4V material. The sheet was formed to a Z-shape and attached with fasteners to the skin at the top and to the lower cap at the bottom. The skin is a continuous sheet with no joints. The overall length of the test area of the specimen is 48.0 in.

A schematic of the test setup is shown in figure 2. The continuous length of the specimen and the loading bar is 141.0 in from pinned end to pinned end. Loads are applied to the specimen at each of the frames through a system of hydraulic jacks located 36.0 in inside the pinned ends. This loading approach results in a constant bending moment applied to the specimen from jack location to jack location. Heating is applied to the top of the specimen (skin side) by a system of radiant heat lamps. Areas other than the 48.0-in test portion are protected from the heating by a system of heat shields.

The basic method of the test is to apply heat to the skin for (1) creating compressive thermal stresses in the skin area and (2) elevating the skin temperature such that creep can occur more readily in the skin. The purpose of the loading system is to cause a compressive stress in the skin area to augment the compressive thermal stresses. The magnitude of the applied load is selected so that the combined mechanical load skin stresses and the skin thermal stresses are of such magnitude that significant creep occurs due to the combination of stress and temperature of the skin.

The specimen was extensively instrumented with strain gages and thermocouples. Strain gages on the skin were arranged in both equiangular rosettes and T configurations so that biaxial stress situations and principal stresses could be accommodated. Strain gages located on the frames were arranged in T configurations so that axial stresses could be measured. Measurement of strain in the temperature environment of the experiment in this paper has traditionally been a problem. Two types of elevated-temperature strain gages were used (foil and weldable types). An extensive investigation of their characteristics is found in reference 4. Chromel-alumel thermocouples were spotwelded at the same locations as the strain gages. The location of the instrumentation is shown in figure 3.

EXPERIMENTAL PROCEDURE

A photograph of the experimental setup is shown in figure 4. A sketch depicting the time histories of a skin and a spar strain gage is presented in figure 5. This sketch is a very comprehensive way to explain the procedure of the experiment in terms of what is happening to the specimen. To follow the experiment's progression, start at the left side of the figure. At this initial time, the heating of the upper skin surface begins. The skin temperature is raised to 825°F and held at this point. Only the upper surface of the skin is heated; as time progresses, heat is transferred to the frames attached to the unheated side of the skin. At some later time, the heat transfer has reached a near steady state, and the thermal stresses (which are causing the early strains) become nontransient. After the thermal stresses are no longer changing with time, loads are applied to the specimen with the system of hydraulic jacks, and a corresponding change in strain is seen. After the loading is completed, the specimen is under stress from two sources: (1) thermal stresses resulting from the nonuniform temperature field and (2) bending stresses resulting from the applied mechanical forces. The object of the experiment is to make the skin creep. The skin is experiencing compressive thermal stresses and compressive bending stresses.

The skin is now at a temperature and stress level such that creep of the skin will begin. The change in strain that occurs is due to creep effects. After approximately 4 hr the load is removed from the specimen and shortly thereafter the heating is terminated. At the far right of figure 5 the specimen has cooled down to room temperature and the strain that remains is a residual, the content of which is discussed in the Results section.

PREDICTIONS

The principal point of study in this paper is the residual stresses in the built-up structure resulting from elevated temperature creep. This residual stress distribution due to creep is at the end of a significant computational chain. The temperature distribution of the structure must be computed before thermal stresses can be calculated. The resulting magnitude of thermal stresses directly affects the amount of creep. This experiment provides measured temperatures, thermal stresses, and residual stresses due to creep. Finite-element computer models were utilized to compute temperatures, thermal stresses, and residual stress due to creep. Since measurements and computations are available throughout the test, the

opportunity existed to examine the relative importance of the components. The models themselves and the computational procedures are discussed in the following sections.

Thermal Model

A two-dimensional model of a portion of the center of the test structure was used for the thermal analysis. The basic conduction model was formed of NASTRAN (ref. 5) CHEXA2 elements, as shown in the cross-sectional representation in the upper part of figure 6. This model has a length of 8 in. A time history of temperature was applied to the model through the grid points located on the upper surface of the skin. This constituted the approach to the basic conduction model.

Radiation elements were added to the model, as shown in the lower part of figure 6. The view factors used for the two small outer bays are identical and the view factors used for the three inner bays are the same. The values of the view factors were obtained from tables and charts in references 6 and 7. These values were then adjusted so that all the area view-factor products divided by the area of the elements were numerically close to 0.99. This was done so that energy lost to space (a specific characteristic of NASTRAN) was minimized. The openings (side and bottom) were closed with radiation closure elements on the model so that nearly all of the radiation exchanges were acountable. An additional parameter greatly affecting the radiation heat transfer is the condition of the surface of the metal that leads to the value for the emissivity. A correct value for the emissivity is critical to the accuracy of the calculation. A value of 0.64 was used and the method of determination is discussed in reference 8.

Convection elements were included to simulate the losses from the vertical elements (spars) of the test structure. Convective heat transfer is, in general, a very complicated phenomenon. This experiment provides no exception since the local circulation of air in the proximity of the surfaces is a function of many variables. The primary tool for adjusting to this circulation with NASTRAN is through the convective film coefficient. A more detailed discussion of the film coefficient for this model may be found in reference 8.

Structural Models

Stresses were calculated by making temperature or load inputs or both to several NASTRAN finite-element models. Four structural models were developed of a symmetrical half of the test specimen. One model was developed as a basic bar model using rods (CROD), bars (CBAR), and shear panels (CSHEAR). Three other models were also developed using triangular (CTRIA2) and quadrangular (CQUAD2) plate elements. The models represent a symmetrical half of the test structure and are shown in figure 7. The bar model was composed of 185 elements. The plate models were established with 324 elements for Model A, 154 elements for Model B, and 404 elements for Model C.

The parent of the plate models is the Model A, with Models B and C being derivatives of the former. The temperature distribution through the depth of the spar is quite nonlinear, hence, it is important to determine how many elements are required to obtain a stable answer. The basic Model A has four elements in the spar depth direction, while Model B has two, and Model C has eight in the spar depth direction. These three models provide sufficient variation of element density in the depth direction to assess the impact on computational accuracy. This assessment is discussed in later sections.

Creep Model

The prediction of the residual stresses due to creep is not as straightforward as predicting temperature and thermal stresses. Software such as NASTRAN (ref. 5) has been available for many years for application to

4

thermal stress problems. The complexity of a closed-loop probelm such as creep has not been specifically addressed in terms of a practical approach. However, a practical approach to computing residual stresses due to creep in a built-up structure using an inelastic strain analogy method is employed in this paper. The mathematics of the analogy in terms of isotropic elasticity (ref. 9) is presented in the following paragraphs to rationalize the approach.

Strain relations.— Strain may be composed of two parts; one part is elastic and the other part is inelastic:

$$\epsilon_{ij} = \underbrace{\epsilon'_{ij}}_{\text{elastic}} + \underbrace{\epsilon''_{ij}}_{\text{inelastic}} \tag{1}$$

Inelastic strains may be composed of several parts, such as a temperature part, a creep part, and a plastic part, in which case

$$\epsilon''_{ij} = \underbrace{\epsilon''_{ijT}}_{\text{temperature}} + \underbrace{\epsilon''_{ijc}}_{\text{creep}} + \underbrace{\epsilon''_{ijP}}_{\text{plasticity}} \tag{2}$$

Elastic strains, for example, the strains that cause stress, may be written as the difference between the total strain and the inelastic strain:

$$\epsilon'_{ij} = \epsilon_{ij} - \epsilon''_{ij} \tag{3}$$

The elastic strain is related to stress through the generalized Hooke's law for isotropic elasticity:

$$\epsilon'_{ij} = \frac{\sigma_{ij}}{2G} - \left[\frac{\nu}{1+\nu}\right]\frac{\sigma}{2G}\delta_{ij} \tag{4}$$

where

$$\sigma = \sigma_{11} + \sigma_{22} + \sigma_{33} \tag{5}$$

and

$$\delta_{ij} = 1 \quad \text{when} \quad i = j$$
$$\delta_{ij} = 0 \quad \text{when} \quad i \neq j$$

The general equation (4) may be rewritten in terms of the right-hand side of equation (3) to include the inelastic strain

$$\epsilon_{ij} - \epsilon''_{ij} = \frac{\sigma_{ij}}{2G} - \left[\frac{\nu}{1+\nu}\right]\frac{\sigma}{2G}\delta_{ij} \tag{6}$$

5

Equations (3) and (4) are the constitutive equations whereby a temperature problem can be formulated

$$\epsilon_{ij} - \epsilon_{ijT}'' = \frac{\sigma_{ij}}{2G} - \left[\frac{\nu}{1+\nu}\right]\frac{\sigma}{2G}\delta_{ij} \tag{7}$$

and similarly a creep problem can be formulated

$$\epsilon_{ij} - \epsilon_{ijC}'' = \frac{\sigma_{ij}}{2G} - \left[\frac{\nu}{1+\nu}\right]\frac{\sigma}{2G}\delta_{ij} \tag{8}$$

The same rationale can be extended to a collective problem of creep and temperature:

$$\epsilon_{ij} - \left(\epsilon_{ijT}'' + \epsilon_{ijC}''\right) = \frac{\sigma_{ij}}{2G} - \left[\frac{\nu}{1+\nu}\right]\frac{\sigma}{2G}\delta_{ij} \tag{9}$$

Equations (7) to (9) lead to several important observations. First, it is obvious that equations (7) and (8) have a form in which they are computationally analogous. This allows the conclusion that a creep problem can be computed as a temperature problem by equating

$$\epsilon_{ijC}'' = \epsilon_{ijT}'' \tag{10}$$

For a temperature problem, the inelastic strain is

$$\epsilon_{ijT}'' = \alpha T \tag{11}$$

Second, equation (9), which states the collective problem of temperature and creep, also provides the basis for the use of finite-element software for a combined temperature and creep analysis in a piecewise linear manner. A piecewise linear analysis of a problem in which temperature and creep effects are present is approached by combining the creep strain ϵ_{ijC}'' at a discrete time t_m into the temperature strains ϵ_{ijT}'' such that a composite inelastic strain is created ϵ_{ijTC}'' such that

$$\left(\epsilon_{ijT}'' + \epsilon_{ijC}''\right)_{t_m} = \left(\epsilon_{ijTC}''\right)_{t_m} = (\alpha T)_{t_m} \tag{12}$$

Equation (12) can be used in conjunction with equations (7) through (9) to form isotropic elasticity relationships.

Computational flow diagram.— Since it was shown that a creep problem can be computed as a temperature problem, the procedure utilizing finite-element structural computer programs will be discussed. The basic problem of computing residual stresses due to creep in a built-up structure is readily suitable to a piecewise linear analysis. This is particularly true if the new, very fast computers are utilized.

A basic flow diagram is presented in figure 8 that illustrates the approach. The necessity for studying creep in an airframe application arises from the presence of elevated temperature. This presence also requires a thermostructural analysis of the airframe. Therefore, the basic sequence begins by utilizing the thermostructural analysis to make the geometric, material, force, and temperature inputs from which element stresses are computed. The element stresses are then input to an appropriate creep law and it is determined which of the elements are creeping. If no elements have temperature and stress combinations that result in creep, then the stresses are static and there is no creep problem. However, if one or more

6

elements are creeping, then an amount of creep strain is computed from the creep law for each element, based on the particular stress and temperature situation for that element. This amount of creep deduced from the creep law is also based on some predetermined time interval of suitable convergence.

The amount of creep strain occurring in each creeping element must then be converted to an equivalent thermal strain αT. This is most easily accomplished by adjusting the coefficient of thermal expansion α for each creeping element. Once this is accomplished, then in the case of a transient problem, different temperatures and forces are resubmitted and a new set of element stresses is computed for comparison with the creep law. Additional creep strains are compiled and reduced to αT inputs so that the cycle can be repeated for more time increments.

This is the process whereby the operating stresses and changes in operating stresses with time are identified. The total residual stresses due to creep at the end of m time cycles is computed from cumulative creep strains of the individual elements. The approach is a single computation where the cumulative individual creep strains are represented by the quantity αT. This is accomplished by first applying a uniform temperature to the structure, then altering the coefficient of thermal expansion of each of the creeping elements such that the alteration of the quantity αT equals the cumulative creep in that element. If a problem entails a large number of creeping elements, much extra labor is needed to produce additional element property and material cards to describe the problem. Problems in which there are very few creeping elements and the elements are discrete, that is, not connected to any other creeping elements, may be approached by altering the temperatures at the boundary of the elements. This will be discussed in some detail in the next section.

Creep law convergence.— A typical creep law (which will be presented in a later section) for the Ti-6Al-4V material was examined for convergence for several computational time increments ranging from 0.5 hr to 6.0 hr. The results are presented in figure 9. A convergence to within 5 percent of the asymptote can be achieved with 1-hr time increments. This result is valid because the material does exhibit the classic primary and secondary creep behavior. The major primary effect does occur within 20 hr of creep initiation. This means that the large numbers (creep strain) should occur early in the problem and the seriousness of the creep should be evident.

RESULTS

There are three areas of considerable scientific interest resulting from this heating and loading of a built-up structure that will be addressed. The prediction of temperatures, thermal stresses, and residual stresses due to creep represent major technological factors pertinent to the future successful development of high-speed airframes. The following three subsections will address these technologies individually.

Temperature

Two time segments were selected in the early, transient part of the experiment to examine the prediction of the temperatures. The time slices at 0.167 hr (10 min) and 0.417 hr (25 min) after the beginning of the heating were selected for analysis. The first time slice corresponds to the early transient heating portion of the test (see fig. 5) and the second time slice occurs just before the point at which the loading begins (fig. 5). The comparisons between the laboratory-measured temperatures and the calculated values are presented in figures 10(a) and 10(b). The comparisons between the measured and computed temperatures are generally quite good. The effect of inaccurate temperatures on thermal stresses is discussed in a later section.

Thermal Stresses

When the object is to predict thermal stresses with finite-element computer programs for a built-up structure, there are three primary considerations. First, the temperature field must be predicted with sufficient accuracy to be compatible with the density of modeling elements and with variations in material properties. The second consideration centers around the fact that pertinent material properties such as elastic modulus, coefficient of thermal expansion, thermal conductivity, radiation, and convective coefficients vary considerably as temperature changes for most aerospace metals. The third consideration concerns selecting the appropriate computer element to accurately represent the structure. It would be inappropriate to select a uniaxial element for a biaxial stress situation. It would also be inappropriate to represent areas of large strain gradients with inordinately large elements that could not represent the local strain distribution. The four structural models (Bar Model and Models A, B, and C) represent a cross section of geometries and elements that should include study material for the first and third considerations above. The second consideration, the accuracy of temperature-dependent material properties, would involve expensive material characterizations and is beyond the scope of the contents of this paper.

The measured stresses are presented in figures 11(a) and 11(b) for the time slices at 0.167 hr (10 min) and 0.417 hr (25 min) elapsed time after the beginning of the heating. The first time slice represents the most transient portion of the time history and the second time slice represents a less transient part of the test. The measured stresses are compared to the two most probable models, the Bar Model and Model A. The computed thermal stresses at the first time slice (11(a)) show the Bar Model thermal stresses to be generally greater than those computed for Model A. The measurements for three out of four spars agree quite closely with the computed Bar Model stresses. The computed stresses at the second time slice (11(b)) indicate a much closer agreement between the two computational models. Most measured stresses exceed the computed values of both models for almost half the data points for the second time slice.

Since the temperature gradient from the top to the bottom of the spars is severe, an evaluation of spar element density in terms of computed thermal stresses was appropriate. The primary reason for having the three plate models (A, B, and C) was to examine the element density effect on computed thermal stresses. This effect is illustrated in figure 12 where the same temperature distribution was applied to all three of the models. Refering back to figure 7, at the line of symmetry the Model A has four spar web elements in the depth direction, Model B has two elements, and Model C has eight elements. The obvious conclusion is that Model B has an inadequate number of spar elements. Models A and C provide close enough agreement to provide adequate information for design and analysis purposes.

Since the design and analysis of an airframe would involve predicted rather than known temperatures, it was of interest to examine how much the computed thermal stresses varied when computed and measured temperatures were input independently. This comparison is presented in figures 13(a) and 13(b) for the two previously defined time slices. Since the measured and computed temperatures were quite close to begin with, it was not totally unexpected that the computed thermal stresses would be quite close. The primary exception was Spar 4 at the second time slice, in which the calculated thermal stresses based on computed temperatures were significantly higher.

Residual Stresses Due to Creep

The strains remaining after the structural loads have been removed and after the structure has returned to room temperature (approximately 7 hr after the test is begun, see fig. 5) are the residual stresses associated with creep. There is a very important aspect of experimental strain measurement that must be clarified regarding the interpretation of strain gage information. A strain gage is a sensor designed to measure elastic strain, that is strain that causes stress. A strain gage that is utilized in an elevated

temperature environment is designed so that when the material to which it is attached thermally expands, the sensor expands along with it without sensing strain. This is referred to as temperature compensation, and deviation from this is referred to as apparent strain. Therefore, the inelastic strains of temperatures are not measured; the sensor only measures those strains caused by restraint of free thermal deformation or strain caused by surface tractions. Strain sensors, however, are not compensated for creep (or for plasticity). Therefore, when a material creeps, the sensor measures strains that are not directly related to elastic stress. The strain in the spar area is

$$\epsilon'_{ij} = \epsilon_{ij} \tag{13}$$

The sensor in this area measures the total strain, which is also the elastic strain, that is the strain that causes stress.

The strain measured in the creeped skin area has all three components of equation (1). The total strain is what the sensor measures in this area:

$$\epsilon_{ij} = \epsilon'_{ij} + \epsilon''_{ijC} \tag{14}$$

It is not known how much of the total strain is the ineleastic component ϵ''_{ijC} and how much is the elastic component ϵ'_{ij}. Therefore, until a creep-compensated strain gage is available, the residues must be interpreted from measurements on parts and components that do not creep. The existence of this problem is the reason the strain measurements used for analysis in this paper are located on the spar webs and lower caps. These areas do not creep, but the response of the structure to creep can be measured by the sensors located in the noncreeping area. The skin strain gage residual (segment C, fig. 5(a)), although known in total magnitude, cannot be interpreted because it is not known how much of the residual is elastic strain and how much of the residual is inelastic creep strain. The spar strain gage residual (segment C, fig. 5(b)) is composed of only elastic strain response to creep of the skin.

Residual stresses in the spars and lower caps are shown for the noncreeping areas of the structure in figure 14. The NASTRAN Model A and the NASTRAN Bar Model were used in conjunction with the inelastic strain analogy method of figure 8 to compute the residual stresses due to creep in the noncreeping areas. The literature was searched for an applicable creep law to be used with this approach. The most suitable creep law was found in reference 10 with the form:

$$Ln\ \epsilon''_{ijC} = -24.09 + 22.54T + 0.000006\sigma^2 + 0.905Ln\ \sigma + 0.433Ln\ t \tag{15}$$

The overall comparison of calculated residual creep stress (in the spars and lower caps) with measured values is shown in figure 15. The dominant observation is that the measured values significantly exceed the predicted values. The implications and significance of this result are addressed in the following section.

DISCUSSION

The basic thrust of this paper has been to examine the use of finite-element techniques to predict temperatures, thermal stresses, and residual stresses due to creep in airframes. Since the prediction of temperature has an impact on the prediction of thermal stress, which similarly has an impact on creep residuals, then the process must be examined from a serial point of view.

The computation of the temperatures from the thermal model is not a pure prediction in the strictest sense. The thermal model was developed in a pseudoempirical sense (ref. 8) since both the convective film coefficient and the emissivity of the model were adjusted so the calculations matched the measured data in a preliminary experiment. However, the development of a thermal model for a new airframe will

undoubtedly be supported with experiments to determine critical items such as emissivities and convective coefficients. The thermal model was shown (fig. 10) to do a very credible job of predicting temperatures in the early, transient part of the experiment. Out of curiosity, the long-term suitability of the model was examined. The comparison of the measured and calculated temperatures 2 1/2 hr after the beginning of the heating is shown in figure 16. This figure shows that for longer times there is a problem with the model in the lower web and cap area. Obviously the heat losses in that area are larger than the model predicts. The flat nature of the prediction in this area implies an association with the convection or radiation elements.

The discussion of the correlation between predicted and measured thermal stresses is centered around model element suitability, element density, and computed temperature discrepancies.

The basic thermal stress situation in the test structure is one of uniaxial stresses in the lengthwise direction of the spars. The experiment was planned this way to eliminate a portion of the variables. Since biaxial stesses are essentially nonexistent for this structure, the uniaxial elements of the Bar Model would be expected to result in computations as appropriate as the biaxial elements of the Plate Models. The comparison between the computed stresses of the Bar Model and the Plate Model A are generally seen to substantiate this (figs. 11(a) and 11(b)). The differences are attributed to node point arrangement and the temperature-averaging effect of the four node points of the plate elements. Plate Model C corresponds closer to the computed values of the Bar Model. However, Model A was shown for comparison purposes because of the practicality of using this model. Final judgments involving modeling techniques must ultimately rest with the prudence of the designer.

The changes in thermal stress distribution resulting from varying the number of elements in the spar web area (fig. 7) clearly show the importance of prudent decisions in element density. The appropriate approach is to logically establish a balance between element density and suitable margins of safety to arrive at an answer that is both safe from a practical point of view and economical from a computational point of view. Model A more likely fits this criteria, although Model C probably provides a more accurate distribution of thermal stress. The web will more likely be designed on a magnitude of maximum stress rather than location of maximum stress.

The substitution of calculated temperatures in place of measured temperatures in the thermal stress exercises indicated little difference in computed values. This was an expected result because the measured and calculated temperatures were quite close. However, the importance of minor temperature inaccuracies cannot be underestimated. This can be illustrated by examining the realtively innocuous temperature excursions of figure 10(b) for Spar 4. The maximum excursions from the calculated values appear to be 105 to 126°F. This excursion has a large impact on the change in thermal stress of Spar 4 (fig. 13(b)) where it can be seen that the maximum thermal stress almost doubles in value when the computed numbers are used. Therefore, it is important to note that minor inaccuracies in temperature distribution can have great impact on thermal stress values.

The comparison of measured and calculated residual stresses due to creep were presented in figure 15. The amount of residual stress measured is significantly more than the analysis method indicates. This is not a comforting trend for designers since the discrepancy is by a factor of from 2 to 3 in many cases. However, the techniques of predicting viscoelastic behavior are anything but straightforward. Coupon tests of samples of the structural material used for the skin of the test structure in this report were subjected to compressive creep tests in reference 11. This document clearly outlines the large variations in creep laws that occur in published literature. Although cyclic creep laws and steady-state creep laws are logically different, there appear to be other undefined variables that affect the definition of creep. The creep laws available for the material (Ti-6A1-4V) are all derived for tensile data. The creeping skin area of the test structure in this experiment is in compression. However, the compression creep tests in reference 11 did not identify this as a cause of the poor correlation. The coupon data actually indicated the reverse, and if

10

used would result in poorer correlation. Recent information (refs. 2 and 12) indicates material thickness to be a major creep variable in addition to temperature, time, and stress. There continues to be evidence that the viscoelastic behavior of the material is the major unknown in the prediction of creep in built-up aircraft structures. The most likely reason for the lack of correlation in figure 15 is a lack of complete definition of the viscoelastic behavior of the Ti-6A1-4V material.

CONCLUDING REMARKS

The design, analysis, and trade study exercises required to produce future high-speed airframes require realistic knowledge of predictive techniques. Temperature, thermal stresses, and residual creep stresses have been studied by comparing laboratory values measured on a built-up titanium structure with values calculated from finite-element models. A two-dimensional finite-element thermal model including conduction, radiation, and convection heat transfer was developed that predicted laboratory-measured transient temperatures very well. The emissivity and convective film coefficient were adjusted to empirical data to refine the thermal model; hence, the thermal calculation was not a pure prediction.

Several finite-element models were utilized to examine the relations between the computational thermal stresses and the thermal stresses measured on the built-up test structure. Element suitability, element density, and computational temperature discrepancies were studied for impact on correlation between measured and calculated thermal stress. Both bar and plate elements were found suitable for the uniaxial stress situation of this built-up test structure. The number of elements in the web area of the spar was critical to accurate thermal stress calculation. The optimum number of elements must be established from a balance between element density and suitable safety margins, such that the answer is acceptably safe yet is economical from a computational viewpoint. Since the computed temperature discrepancies were generally quite small, the difference between thermal stresses computed with measured temperatures and with computed temperatures was also quite small. However, it was noted situations exist where relatively small excursions of calculated temperatures from measured values result in far more than proportional increases in thermal stress values.

The measured residual stresses due to creep significantly exceed the values computed by the piecewise linear inelastic strain analogy approach. The most important element in the computation is the correct definition of the creep law. Available literature revealed such a wide variety of viscoelastic properties that the creep law was considered the major contributor to the discrepancy. Computational methodology advances in predicting residual stresses due to creep requires significantly more viscoelastic material characterization than is currently available.

References

1. Stone, J.E.; and Koch, L.C.: *Hypersonic Airframe Structures Technology Needs and Flight Test Requirements.* NASA CR-3130, 1979.

2. Dixon, S.C.; Tenney, Darrel R.; Rummler, Donald R.; Weiting, Allan R.; and Bader, R.M.: *Structures and Materials Technology Issues For Reusable Launch Vehicles.* 18th Annual Electronics and Aerospace Conference, "EASCON 85," Washington D.C., Oct. 28-30, 1985.

3. Jenkins, Jerald M.; and Montoya, Christopher A.: *Experimental Creep Data for a Built-Up Aluminum/Titanium Structure Subjected to Heating and Loading.* NASA TM-84906, 1983.

4. Jenkins, Jerald M.: *A Study of the Effect of Apparent Strain on Thermal Stress Measurement for Two Types of Elevated Temperature Strain Gages.* NASA TM-84904, 1983.

5. *The NASTRAN® User's Manual.* NASA SP-221(05), 1978.

6. Jakob, Max; and Hawkins, George A.: *Elements of Heat Transfer and Insulation.* Second ed., John Wiley and Sons, Inc., c. 1950.

7. Rohsenow, Warren M.; and Hartnett, James P.: *Handbook of Heat Transfer.* McGraw-Hill Book Co., New York, c. 1973.

8. Jenkins, Jerald M.: *A Comparison of Laboratory Measured Temperatures with Predictions for a Spar/Skin Type Aircraft Structure.* NASA TM-81359, 1981.

9. Wang, Chi-Teh: *Applied Elasticity.* McGraw-Hill Book Co., Inc., New York, 1953.

10. Davis, John W.; and Cramer, Bruce A.: *Prediction and Verification of Creep Behavior in Metallic Materials and Components for the Space Shuttle Thermal Protection System.* NASA CR-2685, 1976.

11. Jenkins, Jerald M.: *Effect of Creep in Titanium Alloy Ti-6A1-4V at Elevated Temperature on Aircraft Design and Flight Test.* NASA TM-86033, 1984.

12. Blackburn, Linda B.: *Creep Testing of Foil-Gage Metals at Elevated Temperature Using an Automated Data Acquisition System.* NASA TM-84634, 1983.

19.15 in

0.97 in

0.93 in

0.250 in

6.00 in

6.00 in

5.25 in

4.00 in

0.050 in

0.450 in

Frame 1   **Frame 2**   **Frame 3**   **Frame 4**

6058
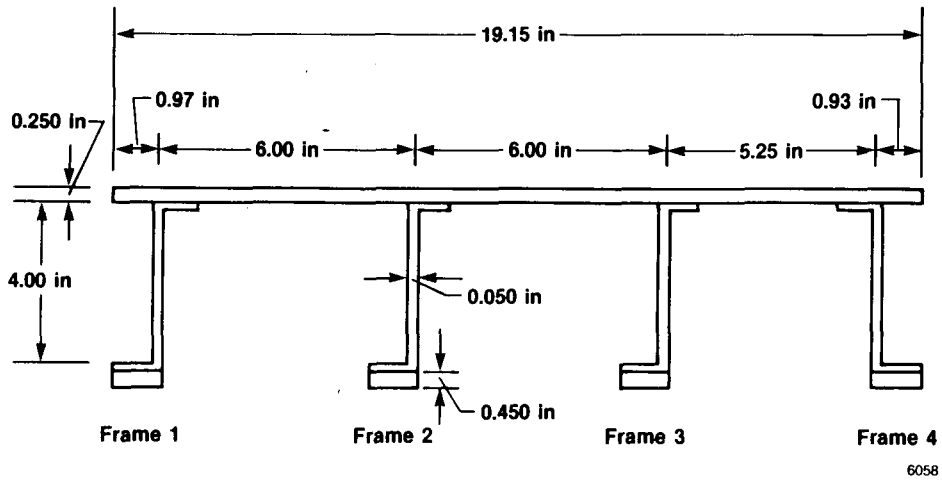
Figure 1. Test specimen cross section.

36.0 in

36.0 in

Centerline

Radiant heater

Heat shield

Heat shield

Loading bar

Specimen

Loading bar

Heated area

48.0 in

Loading mechanism

Loading mechanism

0   36.0 in   46.5 in   70.5 in   94.5 in   105.0 in   141.0 in

Station

6059
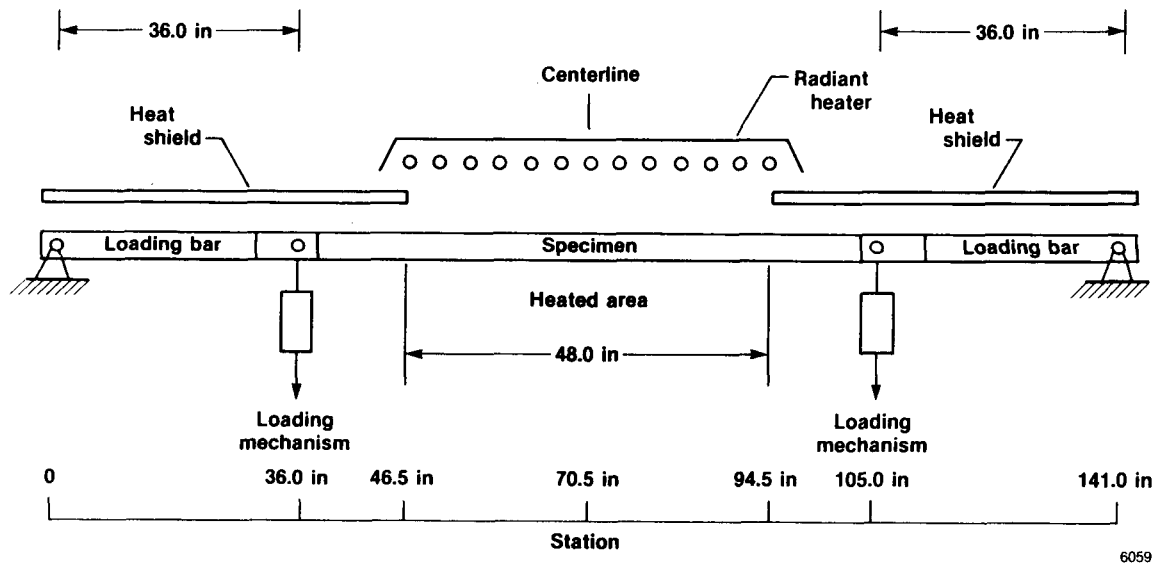
Figure 2. Test setup schematic.
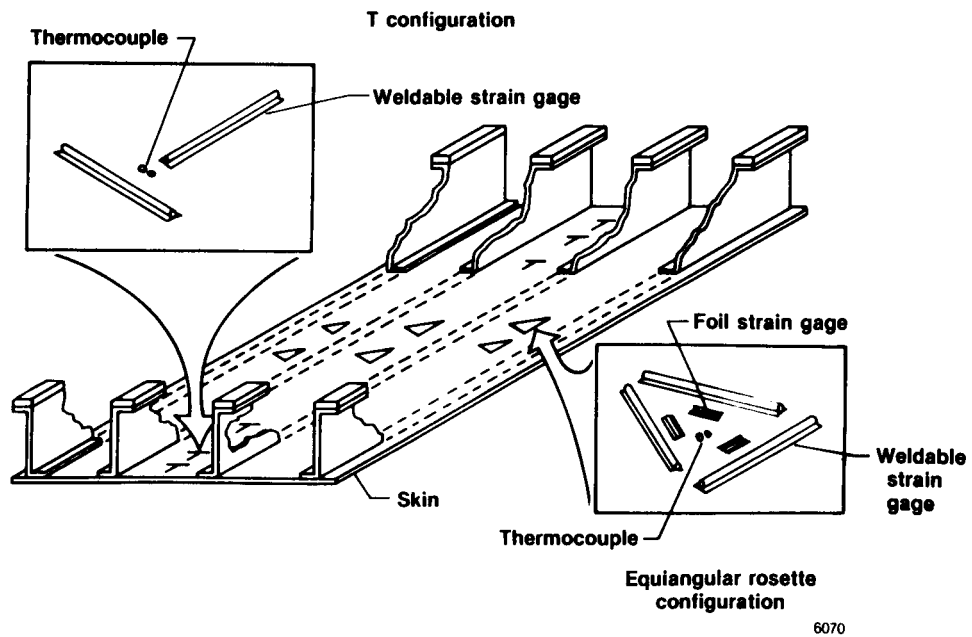
(a) Skin instrumentation.
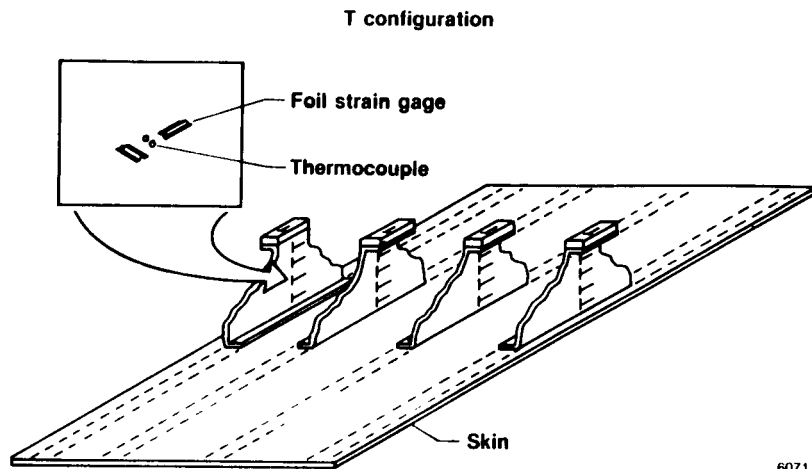
(b) Spar instrumentation.

Figure 3. Strain gage and thermocouple locations on test structure.
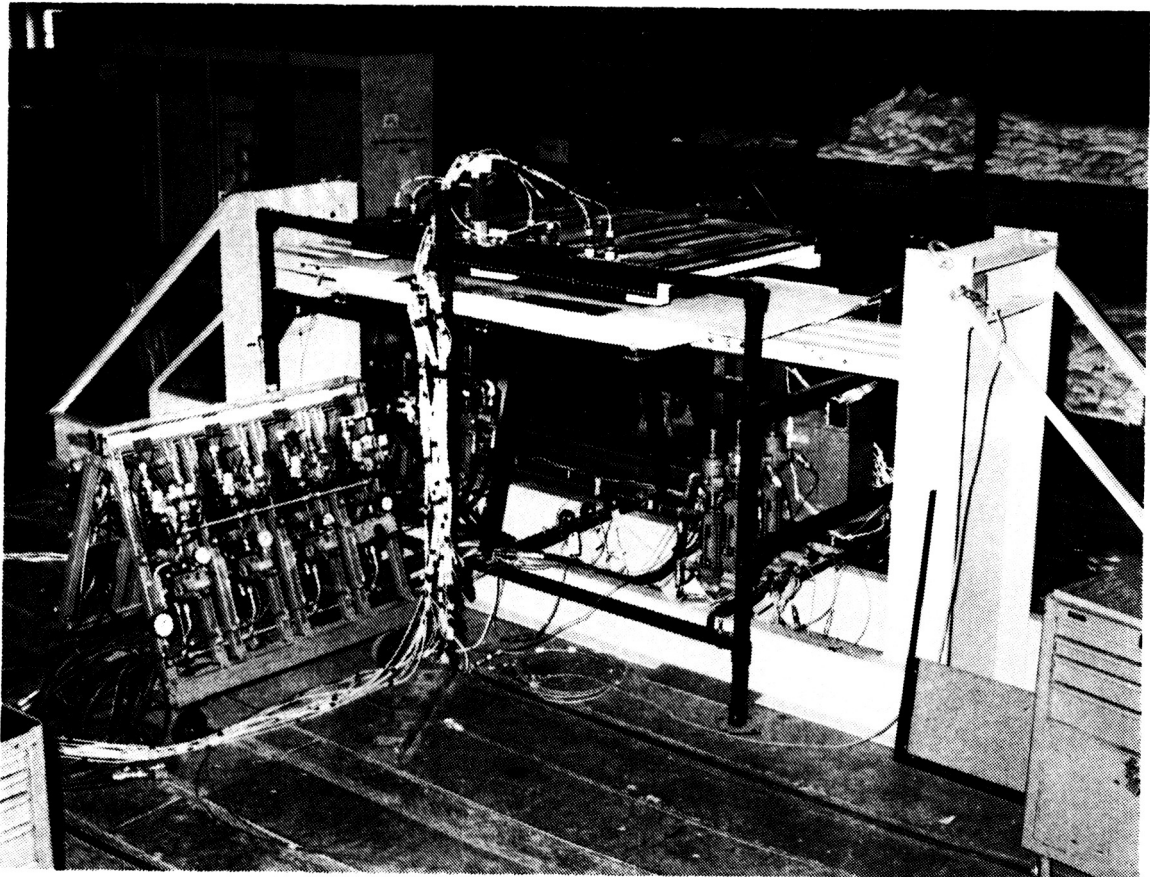
E 39018

Figure 4. Test setup.

(a) Skin strain gage.

Strain, μ in/in

- −1000
- −800
- −600
- −400
- −200

t = 0.167 hr

Viscoelastic response (creeping and relaxing)

Complete loading

t = 0.417 hr

Begin loading

Begin heating

Begin removal of load

Terminate heating

Complete removal of load

t = 6.5 hr

Elastic strain plus inelastic creep strain

Time, hr
0 1 2 3 4 5 6 7

6073
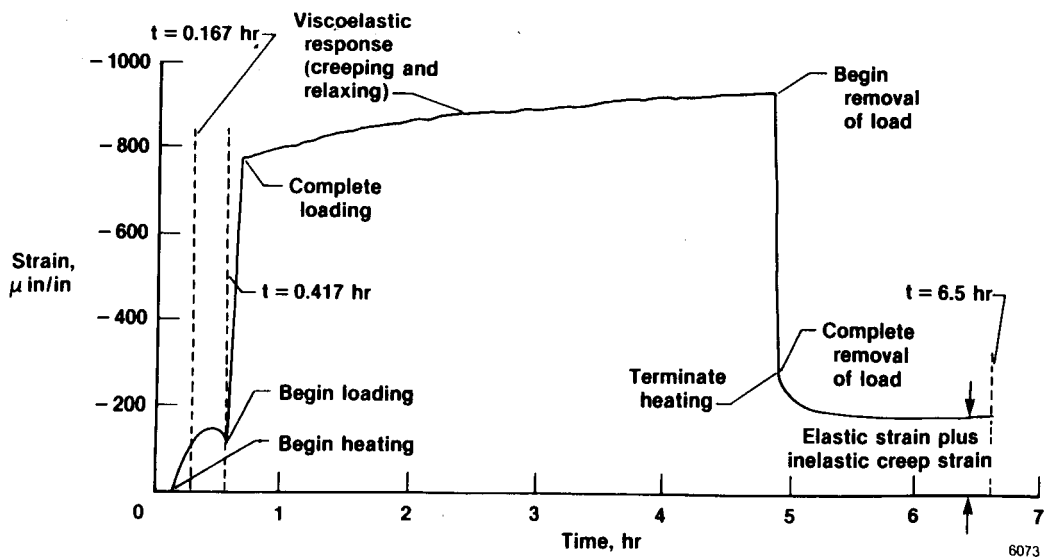
(a) Skin strain gage.

(b) Spar strain gage.

Strain hr/in

- 1500
- 1000
- 500
- 0
- −500

t = 0.167 hr

t = 0.417 hr

Begin loading

Complete loading

Begin heating

Viscoelastic response (relaxation)

Begin removal of load

Complete removal of load

Terminate heating

t = 6.5 hr

Elastic strain

Time, hr
0 1 2 3 4 5 6 7

6074

(b) Spar strain gage.

Figure 5. Anatomy of creep experiment based on strain response.

16
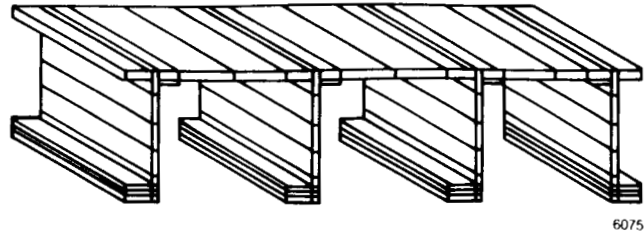
(a) Conduction elements.
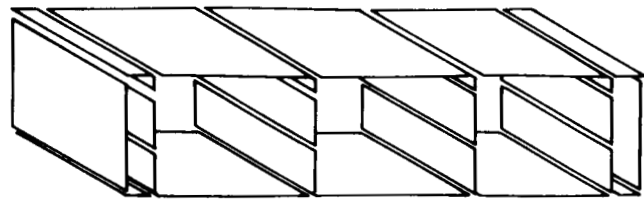
(b) Radiation elements.
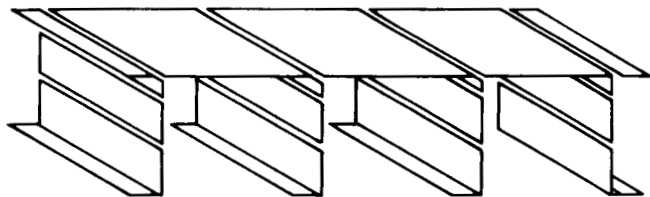
(c) Convection elements.

Figure 6. NASTRAN model used for thermal analysis.
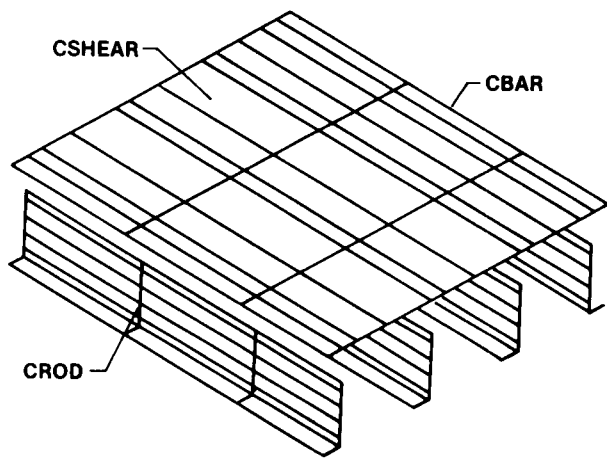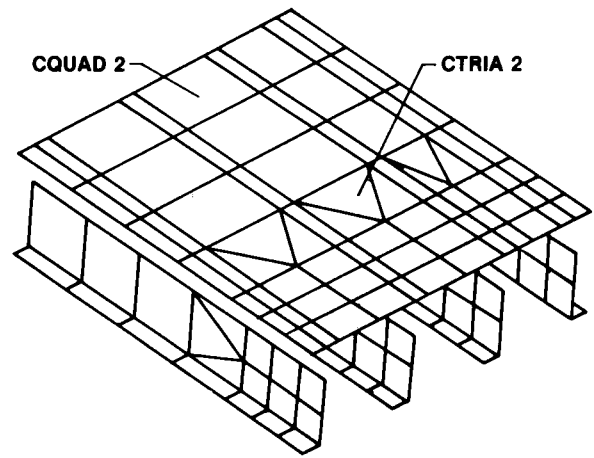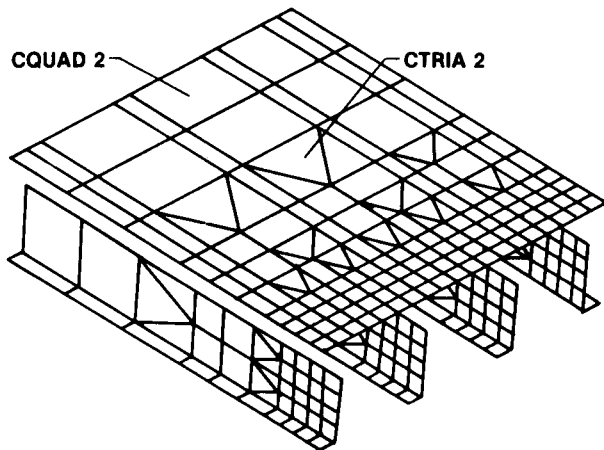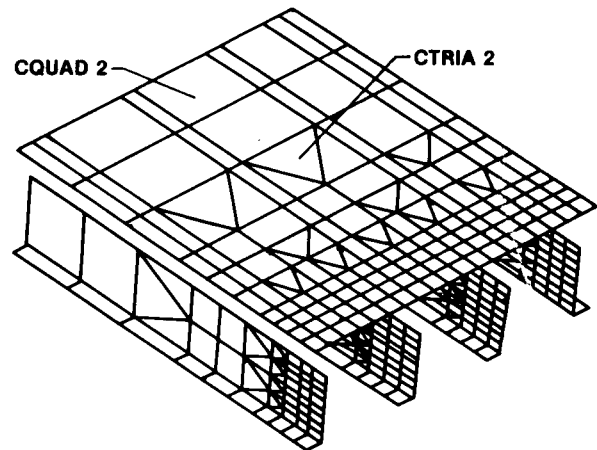
Figure 7. Summary of NASTRAN models used for structural predictions.

18
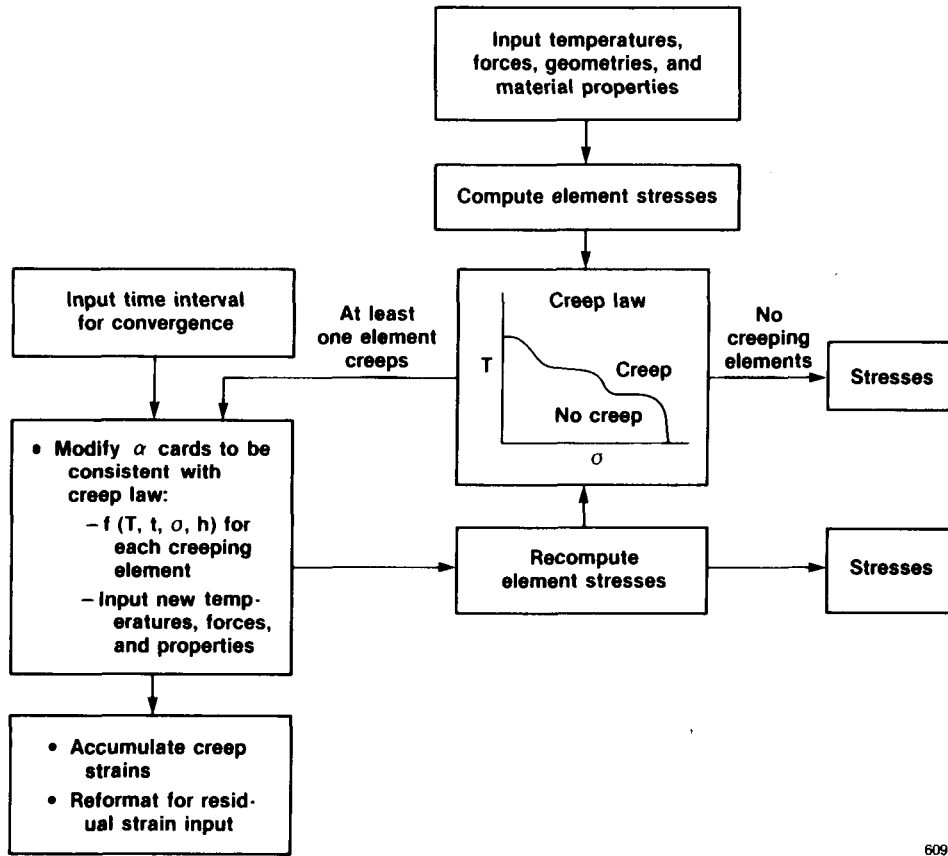
Figure 8. Computational flow diagram.
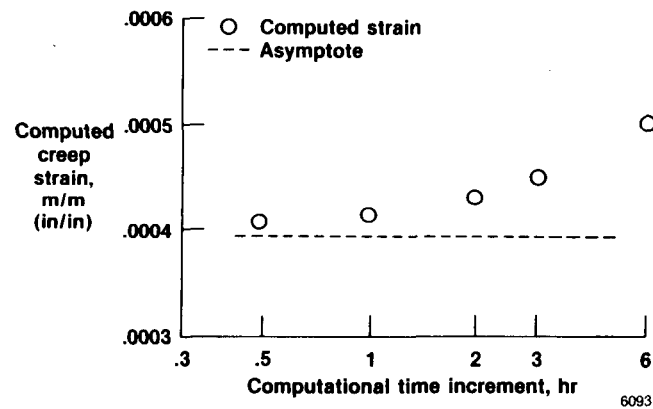
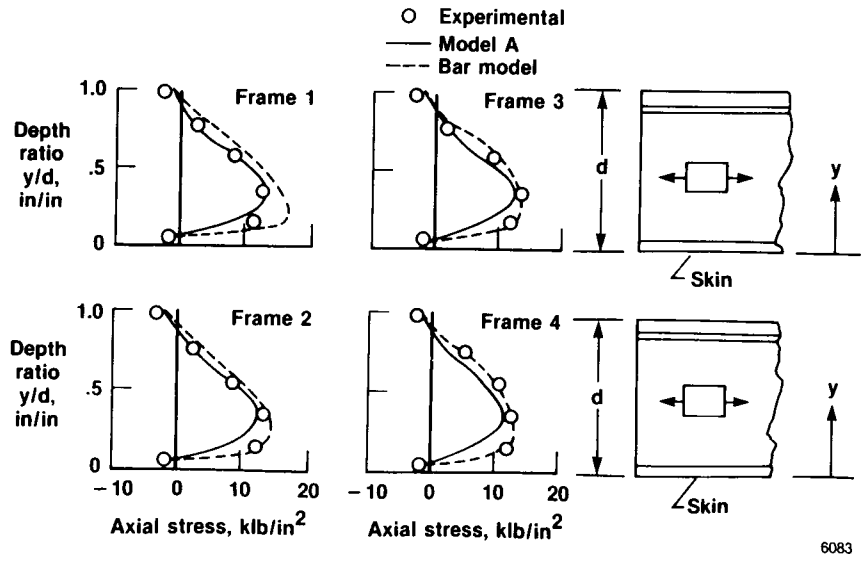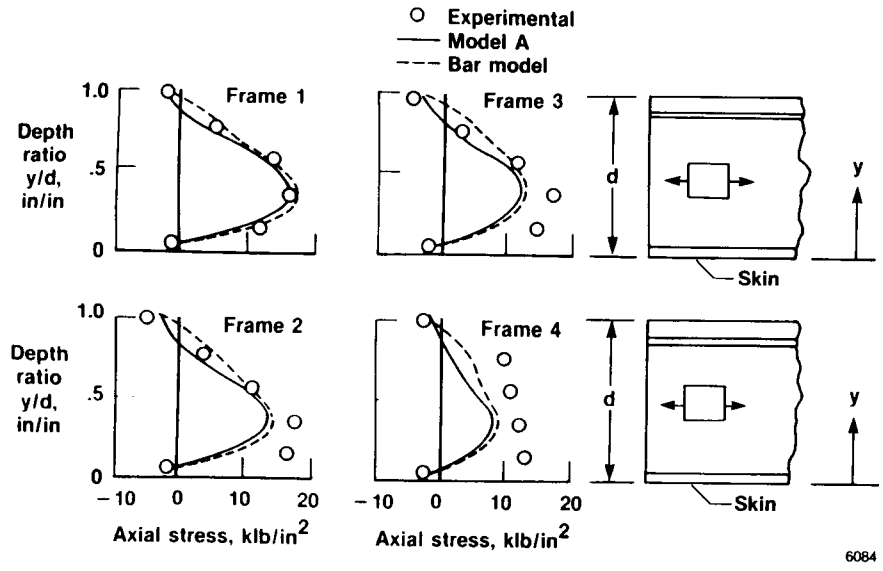*Figure 9. Creep law convergence for several time increments.*

19
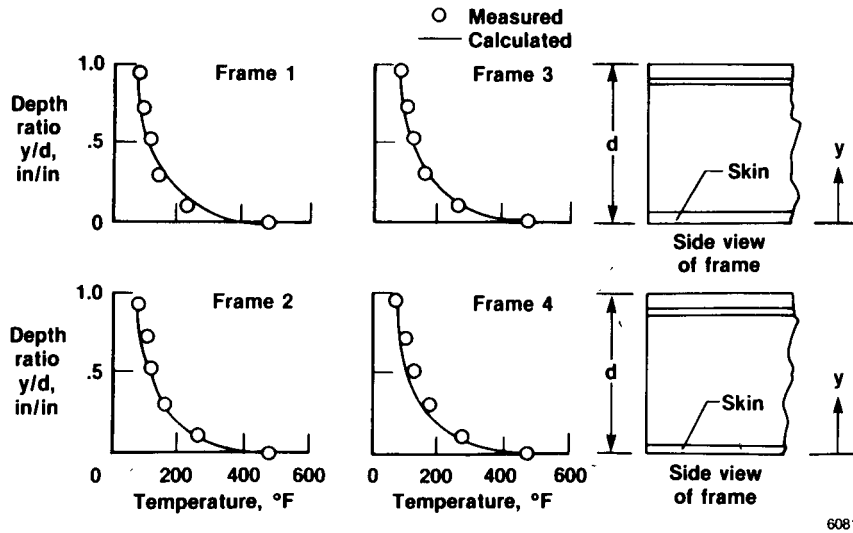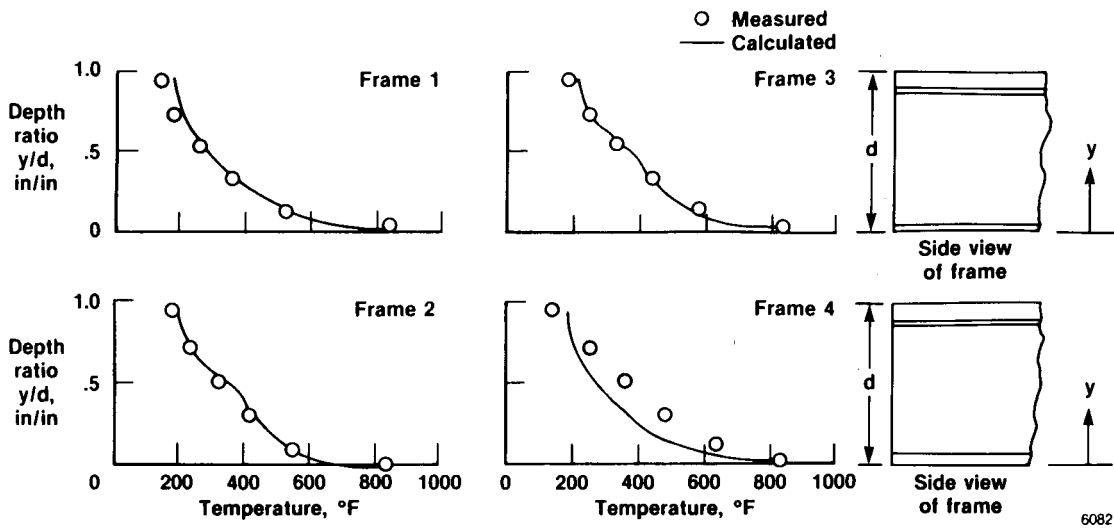
(a) T = 0.167 hr.

(b) T = 0.417 hr.

Figure 10. Comparison of measured and calculated temperatures.

(a) $T = 0.167$ hr.

(b) $T = 0.417$ hr.

Figure 11. Comparison of measured and calculated thermal stresses based on measured temperatures.
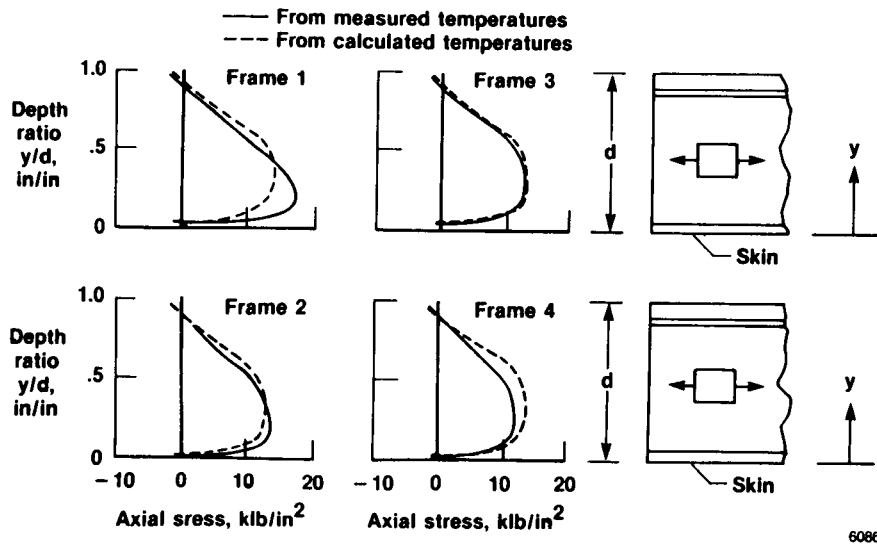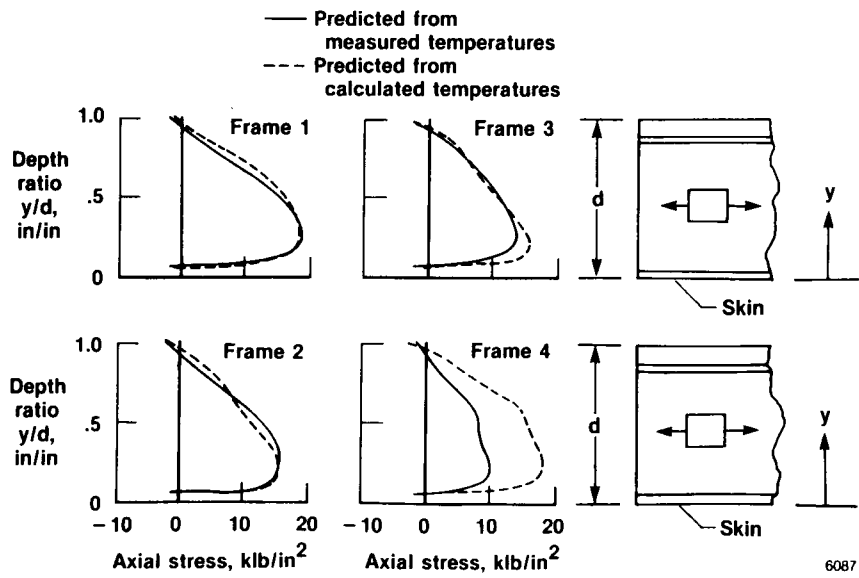
21
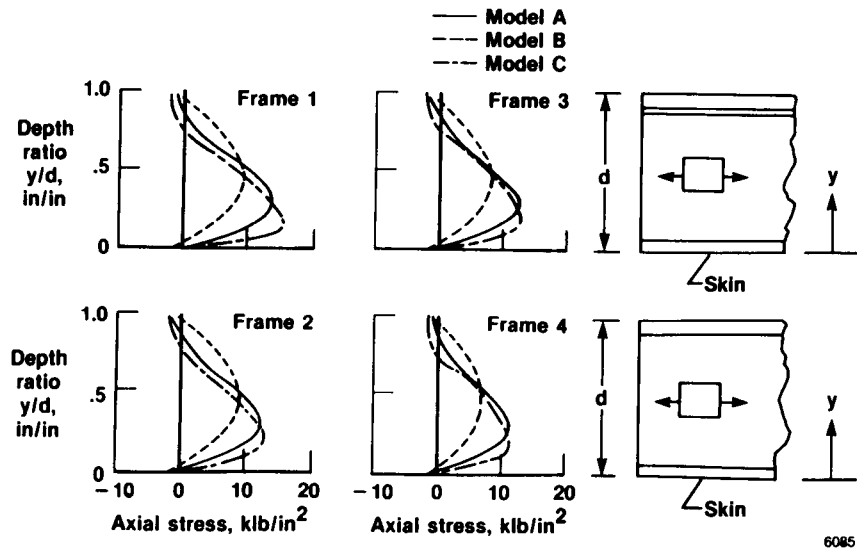
Figure 12. Evaluation of effect of element density on thermal stress distribution for plate models.

(a) T = 0.167 hr.

Figure 13. Comparison of thermal stresses predicted from measured and computed temperatures.

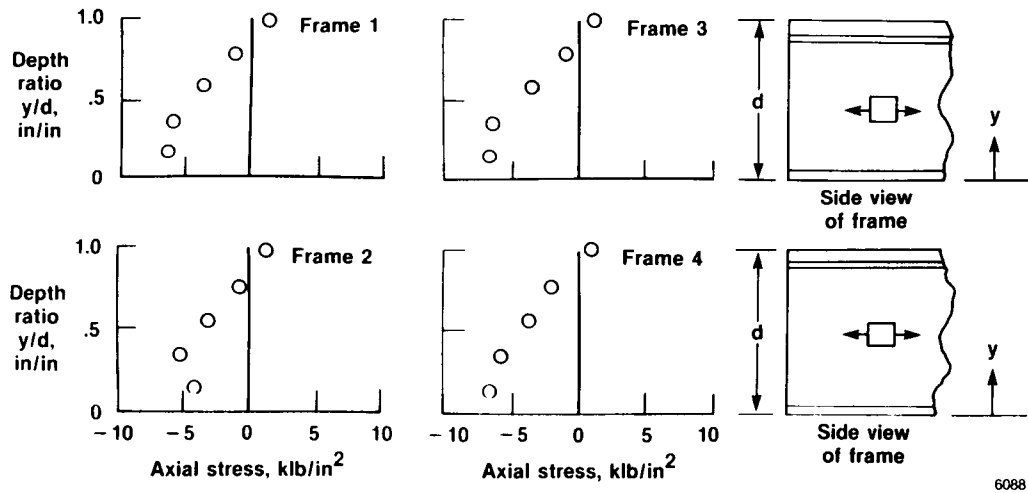*(b) T = 0.417 hr.*

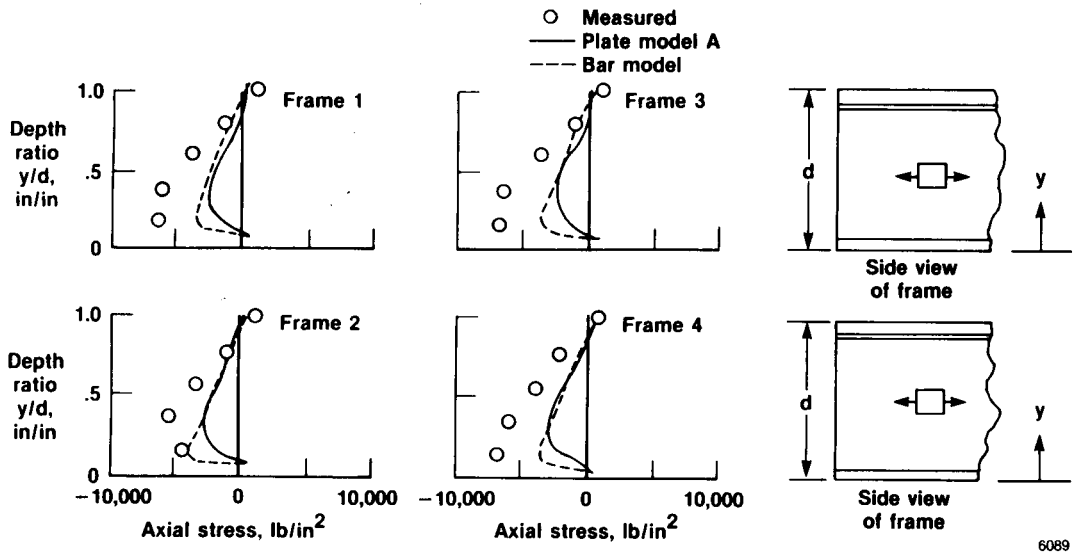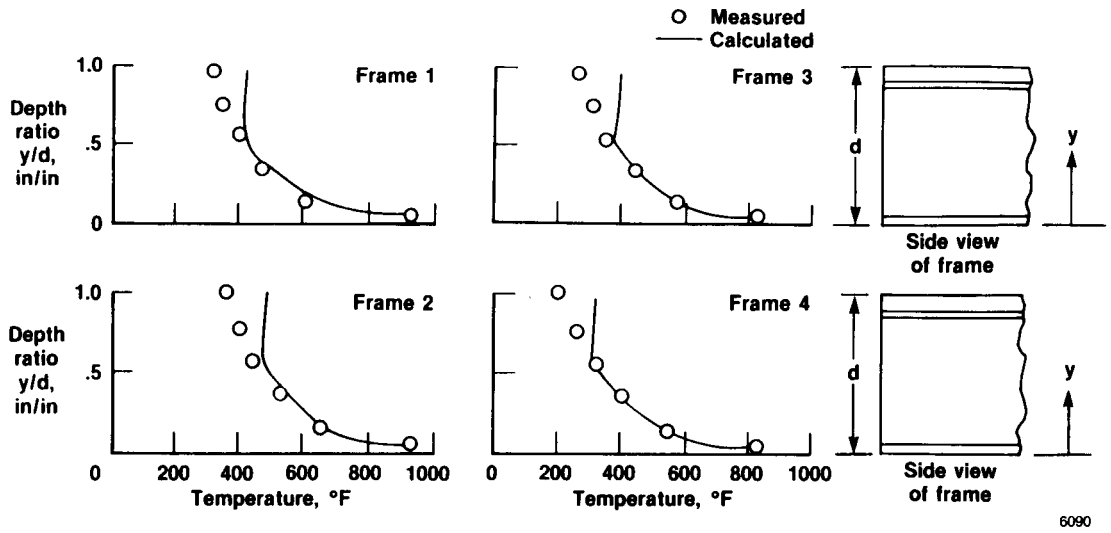*Figure 13. Concluded.*

Figure 14. Measured residual stresses in webs and lower caps.

23

Figure 15. Comparison of measured and calculated residual stresses due to creep, based on measured stresses.

Figure 16. Comparison of measured and calculated temperatures 2 1/2 hr after the heating began.

24

1. Report No. NASA TM-86814	2. Government Accession No.	3. Recipient's Catalog No.
4. Title and Subtitle Comparison of Measured Temperatures, Thermal Stresses and Creep Residues With Predictions on a Built-up Titanium Structure		5. Report Date **November 1987**
		6. Performing Organization Code
7. Author(s) Jerald M. Jenkins		8. Performing Organization Report No. H-1354
9. Performing Organization Name and Address NASA Ames Research Center Dryden Flight Research Facility P.O. Box 273, Edwards, CA 93523-5000		10. Work Unit No. RTOP 506-43-81
		11. Contract or Grant No.
12. Sponsoring Agency Name and Address National Aeronautics and Space Administration Washington, DC 20546		13. Type of Report and Period Covered Technical Memorandum
		14. Sponsoring Agency Code

15. Supplementary Notes

16. Abstract

Temperature, thermal stresses, and residual creep stresses were studied by comparing laboratory values measured on a built-up titanium structure with values calculated from finite-element models. Several finite-element models were used to examine the relationship between computational thermal stresses and thermal stresses measured on a built-up test structure. Element suitability, element density, and computational temperature discrepancies were studied to determine their impact on measured and calculated thermal stress. The optimum number of elements is established from a balance between element density and suitable safety margins, such that the answer is acceptably safe yet is economical from a computational viewpoint. It was noted situations exist where relatively small excursions of calculated temperatures from measured values result in far more than proportional increases in thermal stress values. Measured residual stresses due to creep significantly exceeded the values computed by the piecewise linear inelastic strain analogy approach. The most important element in the computation is the correct definition of the creep law. Computational methodology advances in predicting residual stresses due to creep require significantly more viscoelastic material characterization than is currently available.

17. Key Words (Suggested by Author(s)) Creep Heat transfer Temperature Thermal stress	18. Distribution Statement Unclassified — Unlimited Subject category 39

19. Security Classif. (of this report) Unclassified	20. Security Classif. (of this page) Unclassified	21. No. of Pages 25	22. Price* A02